Vimseltinib: A Precision CSF1R Therapy for Tenosynovial Giant Cell Tumors and Diseases Promoted by Macrophages
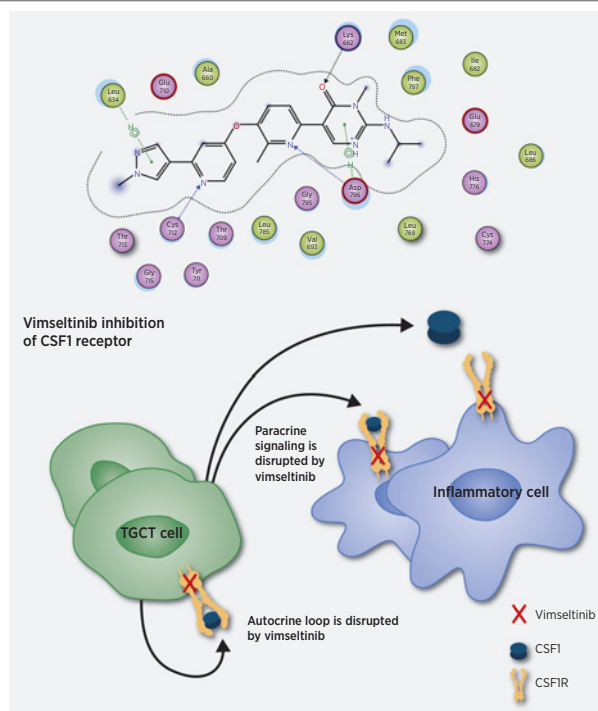
Bryan D. Smith[1], Michael D. Kaufman[1], Scott C. Wise[1], Yu Mi Ahn[1], Timothy M. Caldwell[1], Cynthia B. Leary[1], Wei-Ping Lu[1], Gege Tan[1], Lakshminarayana Vogeti[1], Subha Vogeti[1], Breelyn A. Wilky[2], Lara E. Davis[3], Maitreyi Sharma[1], Rodrigo Ruiz-Soto[1], and Daniel L. Flynn[1]

ABSTRACT

Macrophages can be co-opted to contribute to neoplastic, neurologic, and inflammatory diseases. Colony-stimulating factor 1 receptor (CSF1R)-dependent macrophages and other inflammatory cells can suppress the adaptive immune system in cancer and contribute to angiogenesis, tumor growth, and metastasis. CSF1R-expressing osteoclasts mediate bone degradation in osteolytic cancers and cancers that metastasize to bone. In the rare disease tenosynovial giant cell tumor (TGCT), aberrant CSF1 expression and production driven by a gene translocation leads to the recruitment and growth of tumors formed by CSF1R-dependent inflammatory cells. Small molecules and antibodies targeting the CSF1/CSF1R axis have shown promise in the treatment of TGCT and cancer, with pexidartinib recently receiving FDA approval for treatment of TGCT. Many small-molecule kinase inhibitors of CSF1R also inhibit the closely related kinases KIT, PDGFRA, PDGFRB, and FLT3, thus CSF1R suppression may be limited by off-target activity and associated adverse events. Vimseltinib (DCC-3014) is an oral, switch control tyrosine kinase inhibitor specifically designed to selectively and potently inhibit CSF1R by exploiting unique features of the switch control region that regulates kinase conformational activation. In preclinical studies, vimseltinib durably suppressed CSF1R activity *in vitro* and *in vivo*, depleted macrophages and other CSF1R-dependent cells, and resulted in inhibition of tumor growth and bone degradation in mouse cancer models. Translationally, in a phase I clinical study, vimseltinib treatment led to modulation of biomarkers of CSF1R inhibition and reduction in tumor burden in TGCT patients.

Vimseltinib inhibition of CSF1 receptor

Paracrine signaling is disrupted by vimseltinib

Inflammatory cell

TGCT cell

Autocrine loop is disrupted by vimseltinib

X Vimseltinib

CSF1

CSF1R

[1]Deciphera Pharmaceuticals, LLC, Waltham, Massachusetts. [2]University of Colorado Cancer Center, Aurora, Colorado. [3]Oregon Health & Science University, Knight Cancer Institute, Portland, Oregon.

Corresponding Author: Daniel L. Flynn, Chief Scientific Officer, Research & Development, Deciphera Pharmaceuticals, LLC, 200 Smith Road, Waltham, MA 02451. Phone: 785-830-2115; Fax: 785-830-2150; E-mail: dflynn@deciphera.com

Introduction

Colony-stimulating factor 1 receptor (CSF1R)-dependent macrophages modulate innate and adaptive immunity, as well as tissue repair and homeostasis (1). Cancer and other diseases can usurp these cellular functions into promoting disease. For example, tumor-associated macrophages (TAM) mediate angiogenesis, invasiveness, metastasis, and immunosuppression via secretion of cytokines as well as direct interaction with other cells in the tumor microenvironment (2–5). TAMs can be educated by tumors to express PD-L1, dampening the cytotoxic T-cell immune response (5). Osteoclasts, which derive from CSF1R-dependent monocytes, can be stimulated by tumor cells to degrade bone, allowing for bone invasion and metastasis (6). In the rare disease tenosynovial giant cell tumor (TGCT), the tumor itself consists of macrophages and other CSF1R-dependent inflammatory cells. In a majority of cases, a small number of neoplastic cells within the tumor harbor *CSF1* gene alterations, leading to CSF1 overproduction. High

levels of CSF1 drive the expansion of the tumor mass by recruiting and inducing local proliferation of CSF1R-dependent cells (7, 8).

Small-molecule inhibitors or antibodies targeting CSF1R (or one of its ligands, CSF1) have advanced into the clinic as direct antitumor treatments or potential immunotherapies (9–14). Treatment of cancer with CSF1R inhibitors in combination with immunotherapies has had mixed results, with promising preclinical findings not yet translating to clinical success (15, 16). In contrast, clinical results with CSF1R inhibitors as single agents in TGCT have been quite favorable, with high overall response rates and quality-of-life improvements (9, 11, 17–19). Pexidartinib, an inhibitor of CSF1R, KIT, FLT3, and PDGFRA/B kinases, was recently approved by the FDA for the treatment of TGCT not amenable to improvement with surgery, based on the results of a placebo-controlled, double-blind phase III study (20). The U.S. Prescribing Information for pexidartinib includes a boxed warning of hepatotoxicity and is only available to patients in the United States through a Risk Evaluation and Mitigation Strategy (REMS) Program (20). Although the exact mechanism is unknown, pexidartinib is partially converted to metabolites that may contribute to observed hepatotoxicity (21). In addition, pexidartinib and other small-molecule CSF1R inhibitors also inhibit closely related kinases such as KIT, PDGFRA, PDGFRB, FLT3, and/or other kinases (11, 22–24). Such off-target liabilities may limit the extent of dosing to optimal CSF1R suppression. Selective small-molecule CSF1R inhibitors could be beneficial in TGCT, or in combination with lymphocyte checkpoint inhibitors and/or chemotherapeutic agents in cancer (23).

Vimseltinib was designed to selectively inhibit CSF1R using structure-based drug design and traditional medicinal chemistry approaches. Preclinical data supporting the drug as a potent and selective CSF1R inhibitor, and translational data, including biomarker and promising initial efficacy results in patients with TGCT, are described.

Materials and Methods

Chemicals

Vimseltinib was synthesized as described in U.S. patent 9181223B2, example 10 (25). Pexidartinib was obtained commercially (MedKoo Biosciences, Inc. #206178).

Cell lines and culture conditions

THP-1 (male human acute monocytic leukemia, #TIB-202; RRID: CVCL_0006) and M-NFS-60 (mouse myelogenous leukemia, #CRL-1838; RRID:CVCL_3543) were purchased from the ATCC. Cells were cultured in RPMI1640 media containing 10% FBS, 1% penicillin-streptomycin-L-glutamine, and 0.05 mmol/L 2-mercaptoethanol. M-NFS-60 cells were grown with 20 ng/mL mouse CSF1 (R&D Systems, #416-ML/CF). Cell lines were expanded upon receipt and frozen in aliquots at an early passage number. Cells were then passaged <6 months after resuscitation. The ATCC performs short tandem repeat (STR) analysis for characterization. Further STR characterization was not performed. *Mycoplasma* testing was performed monthly using the MycoAlert Detection Kit (Lonza, Inc, #LT07-318). Human osteoclast precursors were obtained from Lonza, Inc. (#2T-110).

Expression, purification, and crystallization of CSF1R in complex with vimseltinib

CSF1R (residues 542–919, Δ696–741, C677T, C830S, C907T; ref. 26) was cloned into the pEMB44-SapElectra baculovirus expression vector in frame with a N-terminal 6x HIS tag (ATUM). P3/P4 virus stock was produced in SF9 insect cells and large-scale expression of CSF1R was completed in *Trichopulsia ni* (Tni) embryonic cells (Expression Systems). CSF1R was purified by eluting from a Hi-Trap chelating HP column (GE Healthcare) in 20 mmol/L Tris pH 5.0, 250 mmol/L NaCl, 500 mmol/L imidazole and complete EDTA-free protease inhibitor. CSF1R was further purified by eluting with a gradient of 0–1 mol/L NaCl on a heparin column (GE Healthcare) followed by size exclusion (Superdex 75 column, GE Healthcare) in 50 mmol/L HEPES pH 7.5, 200 mmol/L NaCl, 5 mmol/L DTT, and 5% glycerol. A total of 5 µmol/L vimseltinib was included during expression and in all purification buffers. Crystals were grown using vapor diffusion in sitting drops by incubating at 1:1 ratio of 4 mg/mL CSF1R, 0.5 mmol/L vimseltinib with 100 mmol/L Tris-HCl pH 7.7, 18% PEG 800, 100 mmol/L MgCl₂ at 16°C. Crystals were cryoprotected using crystallization solution supplemented with 20% glycerol. X-ray diffraction data were collected at beamline 21-ID-F at the Advanced Photon Source. Data were reduced and scaled using XDS and XSCALE. The structure was solved by molecular replacement using PHASER and a previously solved structure of CSF1R. Ligand restraints were generated with Jligand. The model was a refined using one TLS group per chain in PHENIX and was build using COOT. The structure has been deposited with the Protein Data Bank (PDB ID 7MFC).

Kinase assays

CSF1R phosphorylated on the juxtamembrane domain (JMD) was obtained from Millipore (#14-551). To generate fully phosphorylated CSF1R, JMD phosphorylated CSF1R (3.7 µmol/L) was incubated with 1 mmol/L ATP for 30 minutes at 30°C. Phosphorylation on Tyr-546 (JMD) and Tyr-809 [activation loop (AL)] was confirmed by Western blot analysis using antibodies from Cell Signaling Technology, Inc. (#3083, RRID:AB_1147674 and #3154, RRID:AB_2085231). Kinase activity was determined by following the production of ADP from the kinase reaction through coupling with the pyruvate kinase/lactate dehydrogenase system. In this assay, the oxidation of NADH (resulting in a decrease in absorbance at 340 nm) was continuously monitored spectrophotometrically at 30°C on a plate reader. Assays were conducted in 384-well plates (100 µL final volume) using enzyme, 1.5 units pyruvate kinase, 2.1 units lactate dehydrogenase, 1 mmol/L phosphoenol pyruvate, 0.28 mmol/L NADH, and 1.5 mg/mL PolyEY in assay buffer [100 mmol/L Tris, pH 7.5, 15 mmol/L MgCl₂, 0.5 mmol/L DTT, 0.1% octyl-glucoside, 0.002% (w/v) BSA, and 0.002% Triton X-100]. ATP was added into the assay mixture to start the reaction immediately. Percent inhibition values were obtained by comparison of reaction rates with DMSO controls. IC₅₀ values were calculated from a series of percent inhibition values determined at a range of inhibitor concentrations using Prism software (GraphPad). For off-rate analysis, compound and recombinant CSF1R kinase were added to the reaction mixture. Reaction curves with compound showed time-dependent inhibition. The dissociation rate constant, k_{off}, was calculated by fitting reaction curve data to $[P] = $ vs. t + ((vi-vs.)/k_{obs}) (1-exp(-k_{obs} t)) and $k_{obs} = k_{off} + k_{on}$ x $[I]/(K_i+[I])$ assuming a two-step slow binding mechanism (27). The half-life of the inhibitor/enzyme complex was calculated using $t_{1/2} = (\ln 2)/k_{off}$. For screening of a large kinase panel at 10 µmol/L ATP, assays were performed at Reaction Biology Corp. using published methods (28). Competitive binding assays were performed at DiscoverX Corporation, using published methods (29).

Cell proliferation assays

A serial dilution of test compound in DMSO was dispensed into black, clear bottom, tissue-culture treated plates (Corning) in triplicate. Cells in complete media containing CSF1 (10–1,000 ng/mL) were

added to the plates and the final concentration of DMSO in all assays was 0.5%. Plates were incubated for a total of 72 hours. Viable cells were quantified by addition of a 440 µmol/L solution of resazurin in D-PBS 5 hours prior to the endpoint. Plates were read using an excitation of 540 nm and an emission of 600 nm.

Osteoclast differentiation assay

Cells were thawed into complete media containing 66 ng/mL RANKL (R&D Systems, #6449-TEC/CF) and 33 ng/mL human CSF1 (R&D Systems, #216-MC/CF). A serial dilution of test compound in DMSO was dispensed into black, clear bottom, tissue-culture treated plates in triplicate. Cells (2,500/well) were added to the plates and the final concentration of DMSO was 0.1%. Plates were incubated for 10 days at 37°C. Osteoclast differentiation was detected by measuring tartrate-resistant acid phosphatase activity in cell supernatant using an acid phosphatase detection kit (Sigma, #387). Absorbance was measured on a plate reader at 550 nm.

Enzyme-linked immunosorbent assays

THP-1 cells in complete media were added to a 96-well plate containing diluted compound at 150,000 cells/well. Cells were incubated 4 hours and then stimulated with 25 ng/mL CSF1 for 5 minutes prior to lysis. Phospho-CSF1R in cell lysates was detected using an anti-CSF1R capture antibody (R&D Systems, #MAB3292; RRID:AB_2085247) and an anti-phospho-tyrosine detection antibody conjugated to horseradish peroxidase (Life Technologies, #03-7720; RRID:AB_2532960). For the washout assay, cells were incubated with 1 µmol/L vimseltinib for 2 hours, and then cells were pelleted and washed thrice with complete media. Cells were then incubated for the indicated time and stimulated with 25 ng/mL CSF1 5 minutes prior to lysis.

Whole blood phospho-ERK flow cytometry assay

Human whole blood from a healthy male donor was obtained in K_2EDTA vacutainer tubes. Compound was added to aliquots of 100 µL whole blood and incubated for 4 hours at 37°C. Human CSF1 (10 ng/mL) was added for 5 minutes at 37°C. Red blood cells were lysed and white blood cells were fixed using Lyse/Fix buffer (BD Biosciences, #558049, RRID:AB_2869117) for 10 minutes at 37°C. Cells were treated with permeabilization buffer (BD Biosciences, #558050, RRID:AB_2869118) for 30 minutes on ice. Cells were stored at −80°C overnight. Cells were washed thrice with stain buffer (BD Biosciences, #554656, RRID:AB_2869006) and incubated with PE-conjugated mouse anti-CD14 antibody (BD Biosciences, #555398, RRID:AB_395799) and Alexa647-conjugated anti-phosphoERK1/2 antibody (Cell Signaling Technology, #4284S, RRID:AB_2139964) for 1 hour at room temperature. After washing cells, data were acquired on a C6 flow cytometer (Accuri). A total of 50,000 events for each sample were obtained within a gate for white blood cells defined using side and forward scatter. Median phospho-ERK fluorescence was measured in cells positive for PE fluorescence.

In vitro ADME assays

Cytochrome P450, MDR1 transporter, and plasma protein binding assays were performed at Sekisui Xenotech, LLC. hERG binding was detected using the Predictor hERG fluorescence polarization assays (Life Technologies).

Mouse models

Mouse studies were performed with the approval of the Animal Care and Use Committee of Molecular Imaging, Inc., an Association for Assessment and Accreditation of Laboratory Animal Care (AAALAC) accredited facility, or with Crown Bioscience, Inc. approved by their Animal Care and Use Committee in accordance with the AAALAC. All mice had food and water *ad libitum* and were observed for clinical signs at least once daily. Tumor volume, where applicable, and body weight were measured 2–3 times weekly. Tumor burden (mg) was estimated from caliper measurements by the formula: tumor burden (mg = mm^3) = (length × $width^2$)/2.

For the pharmacokinetic/pharmacodynamic studies, female DBA/1 mice (Taconic) were randomized with mean group body weights on the first day of dosing. Compound was homogenized into a fine suspension in vehicle. For single dose studies, mice were treated with single oral doses as follows: 0.4% hydroxypropylmethylcellulose (HPMC) vehicle, no CSF1 stimulation control ($n = 4$); 0.4% HPMC vehicle, CSF1 stimulation control ($n = 4$), or vimseltinib at 30 or 15 mg/kg + CSF1 stimulation ($n = 28$ each). A second study was performed with vehicle and CSF1 stimulation controls and lower doses of vimseltinib at 7.5 or 3.75 mg/kg + CSF1 stimulation. For "steady-state" dosing studies, mice were treated with six daily oral doses of 0.4% HPMC vehicle, no CSF1 stimulation control ($n = 4$); 0.4% HPMC vehicle, CSF1 stimulation control ($n = 4$), or vimseltinib at 10, 3, or 1 mg/kg + CSF1 stimulation ($n = 32$ each). Fifteen minutes prior to each timepoint, mice were injected intravenously with 1 µg of CSF1 (Life Technologies, #PMC2044). At 2 hours after dose for vehicle and 2, 4, 6, 8, 12, 18, and 24 hours (and 48 hours for the steady-state study) after dose for vimseltinib, plasma and spleens were collected. Plasma samples were analyzed at Xenometrics, LLC. Spleen samples were lysed with TRIzol reagent (Life Technologies, #15596-026). DNA-free total RNA was purified using an RNA purification kit (Life Technologies, #12173-011A) and DNase (Life Technologies, #12185-010). RNA was converted to cDNA using reverse transcriptase (Life Technologies, #4368814). cDNAs for FOS mRNA and 18S rRNA were then quantified with a StepOne qPCR machine and TaqMan Gene Expression reagents (Life Technologies, #4444557, #4319413E, and #Mm00487425.m1). Levels of cFOS were normalized to the 18S control for each sample, then compared to vehicle controls with and without stimulation with CSF1.

For the PC3 peritibial implant bone metastasis study, male nude mice (Hsd:Athymic Nude-Foxn1[nu]; Envigo) were acclimated for 7 days. PC3 cells ($1 × 10^6$) were implanted in the right leg, between the tibia and fibula in serum-free minimum essential media. Mice were randomly assigned into groups based on body weight and treatment began 6 hours after implant. Groups were treated with oral dosing as follows on days 1–32: 0.4% HPMC vehicle control ($n = 20$); vimseltinib 10 mg/kg every day ($n = 20$); or vimseltinib 10 mg/kg twice daily ($n = 20$). Mice were euthanized on day 32 when the vehicle control tumors reached the established tumor volume criteria of 1,000 mm^3. The right hind limbs were imaged using a small animal micro-CT scanner. Images were reconstructed at high resolution (100 µm) and analyzed using Amira 5.2.2 to obtain isosurface volume renderings. Lesions in the hind limb were scored on the basis of a qualitative assessment of lesion size defined by 0: Normal bone; 1: Minimal lesions—some roughening of the isosurface with small areas of apparent bone resorption; 2: Mild—more numerous lesions, significant roughening of the isosurface with full thickness lesions apparent; 3: Moderate—full thickness lesions that are larger and more numerous. 4: Marked—many, large, full thickness lesions with significant distortion of remaining structure and marked bone loss.

For the MC38 syngeneic colorectal cancer study, female C57BL/6 mice (Hsd:Athymic Nude-Foxn1[nu]; Envigo) were implanted subcutaneously in the lower right flank with $1 × 10^6$ cells in PBS. Mice were

randomized and treatments were started when mean tumor size reached 104 mm^3. Groups were treated as follows on days 12–39: 0.4% HPMC vehicle control orally every day; PBS, i.p., twice a week (n = 15); PD1 isotype (Rat IgG2a; BioXCell) 10 mg/kg, i.p., twice a week (n = 15); anti-PD1 (RMP1–14; BioXCell) 10 mg/kg, i.p., twice a week (n = 15); vimseltinib 10 mg/kg orally every day + PD1 isotype (n = 15); and vimseltinib 10 mg/kg orally every day + anti-PD1 (n = 15). Five animals from each group were sacrificed on day 32 for tumor flow cytometry readouts 2 hours after final dose. Tumors were collected and freshly processed using panels for T cells (CD45, CD3, CD4, CD8), macrophages (CD45, CD11b, F4/80), and regulatory T cells (Treg; CD45, CD4, FoxP3) at Crown Bioscience, Inc.

Macrophages in rat tissues

Formalin-fixed, paraffin-embedded (FFPE) organ tissues were obtained from a 2-week rat toxicology study from 5 vehicle-treated and 5 vimseltinib-treated male rats. Sprague-Dawley rats [Crl:CD (SD)] had been treated for 14 days with vehicle control (0.4% HPMC) or vimseltinib 15 mg/kg orally every day at Covance Laboratories, an AAALAC accredited facility. All procedures were in compliance with applicable animal welfare acts and were approved by the local Institutional Animal Care and Use Committee. FFPE slides were stained using CD68 (Abcam, #Ab125212, RRID:AB_10975465) with DAPI counterstain at NovaScreen Biosciences Corporation. Five nonoverlapping image fields were captured using a Vectra system at 20× magnification and analyzed using inForm software. Total cell counts and CD68$^+$ cell densities (cells/mm^2) were determined.

Pharmacokinetic studies

Pharmacokinetic studies in Sprague–Dawley rats and Beagle dogs were performed at Xenometrics, LLC. Xenometrics is an AAALAC-accredited laboratory. Briefly, in crossover pharmacokinetic studies, 3 fasted male rats were given single doses intravenously with 1 mg/kg vimseltinib in 20% Captisol, 25 mmol/L pH 2 phosphate buffer or

orally with 10 mg/kg vimseltinib in 0.4% HPMC. For the dog study, 3 fasted male dogs were given single doses intravenously with 1 mg/kg vimseltinib in 20% Captisol, 25 mmol/L pH 2 phosphate buffer, or orally with 3, 10, or 30 mg/kg vimseltinib in 0.4% HPMC. For both studies, plasma was collected at timepoints of 0, 0.083 (intravenous arm only), 0.25, 0.5, 1, 2, 4, 6, 8, 12, and 24 hours after dose and then analyzed using LC/MS quantitation.

Human subjects

The safety and tolerability of vimseltinib was tested in a phase I/II study, Study DCC-3014-01-001 (NCT03069469). The study was reviewed and accepted by the FDA and Institutional Review Boards at the University of Colorado Cancer Center (Aurora, CO) and Oregon Health & Science University (Portland, OR), and conducted in accordance with the Declaration of Helsinki. Written informed consent was obtained from all patients before study entry. Tumor assessment was done by MRI scans per local assessment using RECIST v1.1.

Results

Switch control binding mechanism

The chemical structure of vimseltinib and the X-ray co-crystal structure of vimseltinib bound to CSF1R are shown in **Fig. 1**, with data collection and refinement statistics presented in Supplementary Table S1. CSF1R is regulated by phosphorylation of an inhibitory switch (JMD) and an activation switch (AL) that induce conformational changes to activate the kinase. In the inactive conformation, Trp-550 from the JMD occupies the third position of the hydrophobic R-spine of the kinase. In this "inhibitory R-spine" state, Phe-797 from the DFG motif of the AL is displaced to a DFG-out conformation, blocking the ATP pocket, and Tyr-809 in the AL binds as a pseudo-substrate, blocking access to the CSF1R substrate pocket (Supplementary Fig. S1A). Collectively, these conformational effects render CSF1R inactive. Upon ligand binding and receptor dimerization, Tyr residues
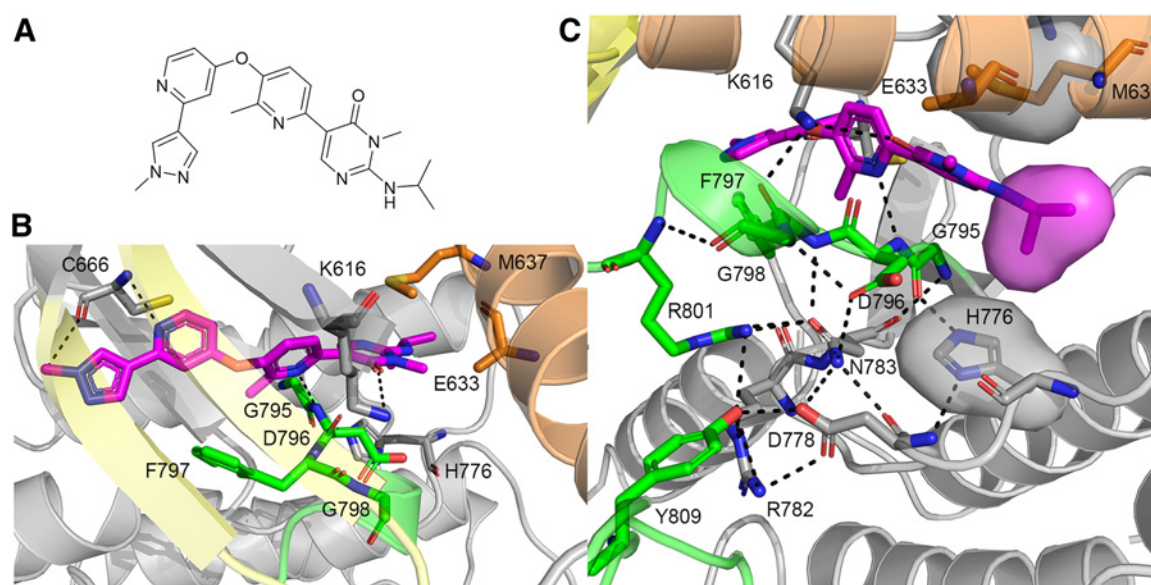
Figure 1.
Structure of vimseltinib. **A,** Chemical structure of vimseltinib. **B,** Cocrystal structure of vimseltinib bound to CSF1R. Direct inhibitor hydrogen bonds with CSF1R. **C,** Nucleation of hydrogen bond network stabilized by vimseltinib binding. PDB:7MFC, (resolution 2.8 Å).

in the JMD are autophosphorylated, dislodging the inhibitory JMD switch including Trp-550. Phe-797 in the AL moves to occupy the third position in an "activated R-spine," which exposes the ATP pocket. Tyr-809 is dislodged from its inhibitory pseudo-substrate conformation, allowing substrate binding and properly orienting catalytic residues required for phosphate transfer. Tyr-809 of the AL can also be autophosphorylated, further stabilizing the AL in the active conformation, but this is not required for kinase activity. Because the pocket in the kinase spine is occupied by either the inhibitory JMD switch or the AL switch, this pocket and proximal AL and catalytic amino acid residues are collectively referred to as the "switch control" region. This region is exploited by vimseltinib to induce CSF1R into an inactive conformation.

An unphosphorylated form of CSF1R was used for crystallization of vimseltinib (chemical structure shown in **Fig. 1A**). Direct interactions of vimseltinib with CSF1R are shown in **Fig. 1B**. The N-isopropyl group of the pyrimidinone ring occupies the switch pocket, serving as a surrogate for the JMD Trp-550 at the third position of the inhibitory R-spine, forcing the displacement of Phe-797 to the DFG-out conformation (**Fig. 1C**; Supplementary Fig. S1B). The pyrimidinone ring breaks the conserved salt bridge of Glu-633 and Lys-616 that is essential for catalysis. Density for the side chain of Glu-633 is not observed because of this disruption. Instead, the carbonyl of the pyrimidinone ring forms a hydrogen bond with Lys-616. The ring nitrogen of the central pyridine ring forms a key hydrogen bond to the backbone NH of Asp-796 of the DFG motif, further stabilizing the AL switch in the off state. CSF1R has Gly-795 preceding the DFG motif, unlike other kinases in its family which have a larger Cys. The 6-methyl group of the central pyridine ring occupies this Gly-795 "hole" in CSF1R that would sterically clash with the Cys side chain in KIT, PDGFRA, PDGFRB, and FLT3, providing selectivity versus these kinases (Supplementary Fig. S2). A similar strategy for selectivity by exploiting the Gly-795 hole has been reported previously (30). Met-637 in the switch pocket also provides an opportunity to engineer CSF1R selectivity. The sulfur atom of Met-637 forms a directed orbital overlap with the pyrimidinone ring. The combination of Gly-795 and Met-637 are only found together in 11 human kinases, and these interactions are proposed to account for a significant component of the kinome selectivity exhibited by vimseltinib. The 6-methyl group, along with the adjacent hinge-binding pyridine ring, form van der Waals interactions with Phe-797 of the DFG, further stabilizing the AL switch in its inactive conformation. Finally, vimseltinib forms a hydrogen bond from the hinge-binding pyridine nitrogen lone pair to the backbone NH of Cys-666, while the pyrazole ring forms electronic interactions with the side chain phenol of Tyr-665 and the pyrazole methyl substituent forms a C-H hydrogen bond with the backbone carbonyl of Cys-666. In composite, these interactions stabilize CSF1R in the inactive conformation, both antagonizing the AL switch from occupying the switch pocket, as well as serving as an agonist for stabilizing the AL switch in its inactive conformation. A similar switch control inhibition strategy has been used for other kinases including KIT, ABL, MET, and p38 (27, 31–33).

Vimseltinib reinforces the inactive conformation of CSF1R through biomimetic nucleation of an array of 17 hydrogen bonds comprised of the CSF1R catalytic amino acid machinery (**Fig. 1C**; Supplementary Fig. S1). Direct inhibitor hydrogen bonding between Lys-616 and the inhibitor pyrimidinone carbonyl and between the central pyridine ring N and the backbone NH of Asp-796 facilitate a hydrogen bond network involving, His-776, Asn-783, Asp-778, Arg-782, Gly-795, Asp-796, Phe-797, and Arg-801. This extended hydrogen bond collapse network locks the catalytic amino acids into an inactive

state and further culminates in the docking of the side chain of Tyr-809 from the AL as an inhibitory pseudosubstrate. The binding of the inhibitor isopropyl group into the third position of the spine stabilizes an extended inhibitory R-spine comprising His-776, Met-683, and Leu-695.

Kinase selectivity and biochemical characterization

CSF1R has at least three distinct phosphorylation states—an auto-inhibited/unphosphorylated form, a phosphorylated JMD form that is catalytically active, and a fully JMD and AL phosphorylated form that further stabilizes the kinase in an active conformation. Kinase inhibitors have different affinity for these states, thus the potency of vimseltinib for all three forms of CSF1R was explored. First, utilizing a continuous spectrophotometric assay, recombinant CSF1R kinase (phosphorylated only on the JMD or fully phosphorylated on the JMD and AL) were tested. Vimseltinib exhibited an approximately 100-fold preference for CSF1R phosphorylated only on the JMD ($IC_{50} = 2.8$ nmol/L) versus fully phosphorylated CSF1R ($IC_{50} = 290$ nmol/L). Unphosphorylated CSF1R is catalytically inactive, thus an *in vitro* binding assay was performed. Vimseltinib exhibited approximately 20-fold weaker affinity for unphosphorylated CSF1R ($K_d = 79$ nmol/L) versus the JMD phosphorylated form ($K_d = 3.6$ nmol/L), presumably due to having to compete with Trp-550 from the JMD for binding in the unphosphorylated form. Inhibition of CSF1R by vimseltinib is insensitive to ATP concentration (Supplementary Fig. S3A). Type II kinase inhibitors induce significant conformational changes upon kinase binding and can exhibit slow-binding kinetics. Using a rapid dilution assay, vimseltinib was found to have an off-rate of 0.0041/minute from CSF1R, corresponding to a half-life of 170 minutes for inhibition (Supplementary Fig. S3B). The final dissociation constant calculated from this experiment ($K_d = 2.3$ nmol/L) was in agreement with data from CSF1R activity and binding assays.

To determine the selectivity for CSF1R kinase, vimseltinib was profiled versus a total of approximately 300 human kinases at 10 μmol/L ATP. Kinases inhibited within 1,000-fold of CSF1R were further tested at cellular levels of ATP (1–4 mmol/L). A kinome tree is shown in Supplementary Fig. S4. Vimseltinib was >100-fold selective for CSF1R versus all kinases tested and >1,000-fold selective for 294 kinases in this panel. Importantly, vimseltinib was >500-fold selective versus FLT3, KIT, PDGFRA, and PDGFRB. Pexidartinib inhibited the JMD phosphorylated form of CSF1R ($IC_{50} = 2.2$ nmol/L) with similar potency to vimseltinib, but also inhibited FLT3, KIT, PDGFRA, and PDGFRB within 5-fold of the IC_{50} for CSF1R (Supplementary Table S2).

Cellular activity of vimseltinib

Vimseltinib was a potent inhibitor of CSF1-stimulated phosphorylation of CSF1R in the human THP1 mononuclear cell line with $IC_{50} = 19$ nmol/L, similar to the potency of pexidartinib ($IC_{50} = 17$ nmol/L). To examine the effects of the long residency time of vimseltinib for CSF1R kinase in cells, a "washout" experiment was performed, wherein THP1 cells were incubated with compound and then washed with media several times. At various timepoints after washout, CSF1R phosphorylation was measured by ELISA. Vimseltinib inhibited CSF1R phosphorylation by approximately 50% 6 hours after washout and approximately 30%–40% at 24 hours (**Fig. 2A**), indicating a long residency time when bound to CSF1R, in agreement with kinetic experiments *in vitro*.

Vimseltinib inhibited proliferation of M-NFS-60 cells, a mouse myelogenous leukemia cell line that requires CSF1 for cell proliferation (11), with an $IC_{50} = 10.1$ nmol/L (**Fig. 2B**). High concentrations of
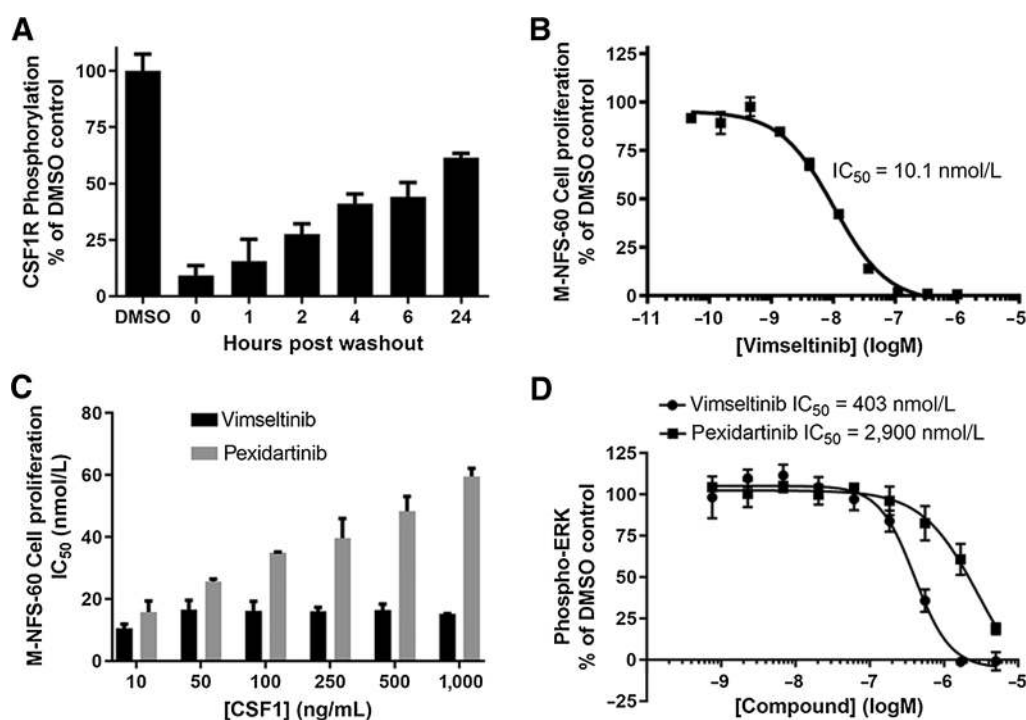
Figure 2.
Cellular activity of vimseltinib. **A,** Time course of inhibition of CSF1R phosphorylation in THP1 cells after compound washout. Cells were treated with 1 µmol/L vimseltinib for 2 hours prior to washout. CSF1R phosphorylation was detected by ELISA. **B,** Inhibition of M-NFS-60 cell proliferation. **C,** Effect of CSF1 ligand concentration on inhibition of M-NFS-60 cell proliferation by vimseltinib and pexidartinib. **D,** Inhibition of CSF1-stimulated phosphorylation of ERK downstream of CSF1R signaling by vimseltinib and pexidartinib in human whole blood.

growth factor ligands for receptor tyrosine kinases can reduce the potency of kinase inhibitors due to increased ligand-induced dimerization and activation of the kinase (34). However, high levels of the CSF1R ligand, CSF1, had only small effects (≤1.6-fold) on inhibition of M-NFS-60 cells by vimseltinib (**Fig. 2C**). Pexidartinib had 3.8-fold less potency at 1,000 ng/mL versus 10 ng/mL CSF1. Pexidartinib has greater affinity to the autoinhibited, JMD bound state (11), which may be less accessible with greater ligand binding and CSF1R dimerization.

Human osteoclast precursors are dependent upon CSF1-stimulated CSF1R activity for proliferation and differentiation into osteoclasts, which are cells that function in bone resorption or bone degradation in osteolytic cancers. Osteoclast differentiation was detected by measuring levels of tartrate-resistant acid phosphatase activity in the supernatant of assay wells. Vimseltinib blocked osteoclast differentiation with $IC_{50} = 9.3$ nmol/L (Supplementary Fig. S5).

To examine vimseltinib inhibition of CSF1R in human primary monocytes, a whole blood assay was performed. Vimseltinib was incubated *ex vivo* with peripheral blood, and CSF1R signaling was stimulated with the ligand CSF1. Levels of phosphorylated ERK (downstream of CSF1R activation) were measured in monocytes using flow cytometry. Vimseltinib inhibited CSF1R signaling in monocytes in human whole blood with an average $IC_{50} = 403$ nmol/L (**Fig. 2D**). Using an *in vitro* ultracentrifugation assay, vimseltinib was found to be approximately 96.5% bound to proteins in human plasma. Correcting the whole blood IC_{50} value for the amount of free drug leads to an adjusted free $IC_{50} \sim 14$ nmol/L, in close agreement with inhibition of CSF1R in cellular assays. Pexidartinib was a weaker inhibitor in this

whole blood assay with $IC_{50} = 2,900$ nmol/L, likely reflecting its higher plasma protein binding (>99% bound).

Pharmacokinetic/pharmacodynamic evaluation of vimseltinib in mice

Pharmacokinetic/pharmacodynamic analysis of vimseltinib inhibition of CSF1R was determined by following CSF1-stimulated cFOS mRNA modulation in mouse spleens (35). Vimseltinib significantly inhibited CSF1-stimulated expression of cFOS mRNA for > 24 hours post dose after single doses of 3.75 to 30 mg/kg (Supplementary Fig. S6). Inhibition of cFOS mRNA expression by 70% to 87% for the entire 24 hours period examined after dose was achieved at 3.75 mg/kg, with an $AUC_{0-24} = 28,987$ ng*hour/mL. Vimseltinib was next evaluated in the same pharmacokinetic/pharmacodynamic model, with six daily oral doses to achieve steady-state plasma levels prior to sampling. Vimseltinib significantly inhibited cFOS expression at doses of 1, 3, and 10 mg/kg (**Fig. 3A**). After dosing at 3 mg/kg, vimseltinib inhibited cFOS expression by 90% or greater for 12 hours, and approximately 50% at 24 and 48 hours. The AUC_{0-24} for the 3 mg/kg group was 49,314 ng*hour/mL (**Fig. 3B**). The maximum concentration (C_{max}) and AUC values were dose proportional. EC_{50} and EC_{80} values calculated for all animals in the study were 430 and 1,700 ng/mL, respectively (**Fig. 3C**). Vimseltinib is approximately 97.2% bound in mouse plasma, thus the free EC_{50} value was 12 ng/mL (28 nmol/L), in agreement with cellular IC_{50} values.

In vivo inhibition of bone degradation in mice

In a PC3 prostate cancer peritibial implant xenograft model in nude mice, mice were treated with vimseltinib at 10 mg/kg, administered
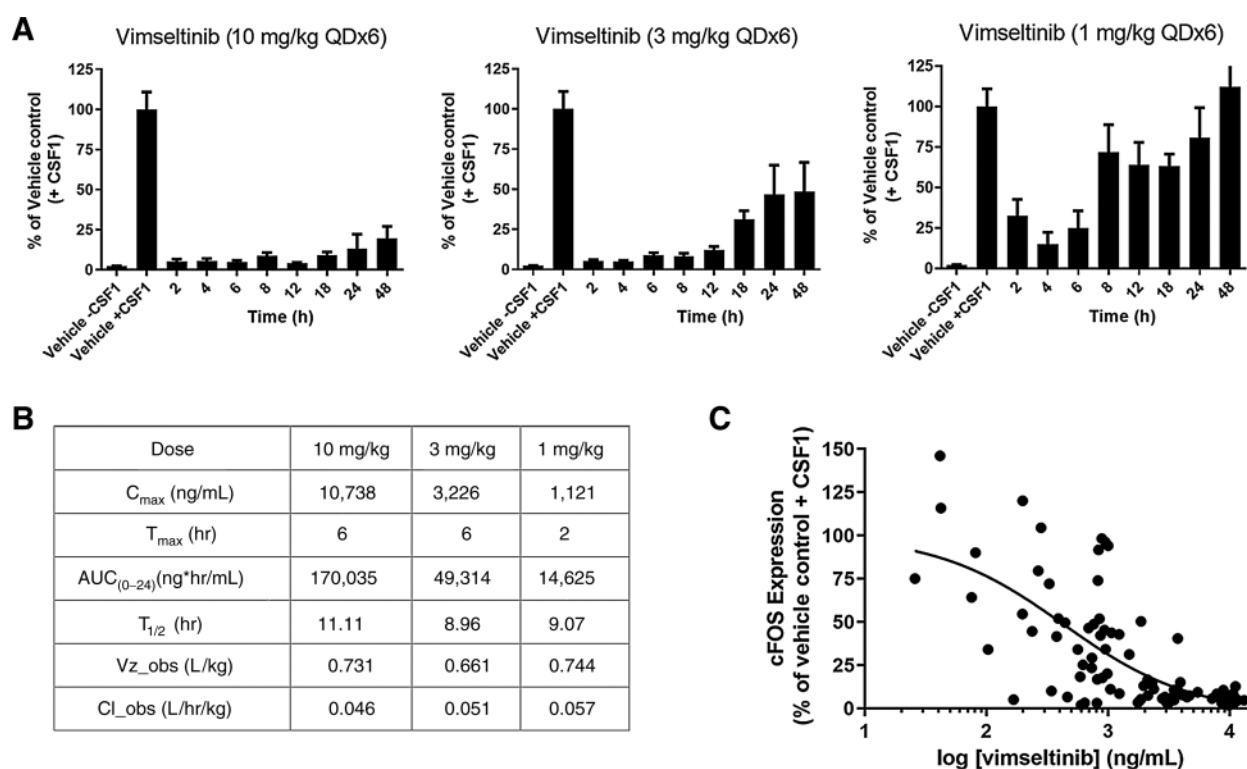
Figure 3.
Pharmacokinetics/pharmacodynamics of vimseltinib in a mouse model. **A,** Steady-state inhibition of CSF1-stimulated cFOS expression after 6 days of oral dosing. **B,** Pharmacokinetic parameters of vimseltinib at steady state in mice. $AUC_{(0-24)}$ = area under the plasma concentration–time curve from 0–24 hours; Cl_obs = total body clearance; C_{max} = maximum concentration; T_{max} = time to maximum concentration; $T_{1/2}$ = half-life; Vz_obs = volume of distribution. **C,** Plot of individual mouse spleen cFOS expression versus vimseltinib plasma concentration, with EC_{50} = 430 ng/mL.

either once or twice daily on days 0 through 32 (until the average vehicle primary tumor reached 1,000 mm³ in size). Both regimens led to statistically significant protection from bone degradation. Representative CT images are shown of the right hind limbs from 2 vehicle-treated mice and 2 mice treated with vimseltinib at 10 mg/kg every day (**Fig. 4A**). Bone degradation scores for 20 mice in each

treatment group were qualitatively scored from 0–4 (**Fig. 4B**). Both every day and twice daily dosing regimens performed similarly in this analysis and had statistically significant bone protection compared with vehicle treatment. Vehicle-treated mice lost weight in this model over time, likely reflecting disease burden (Supplementary Fig. S7A). Both vimseltinib-treated groups had reduced weight loss compared
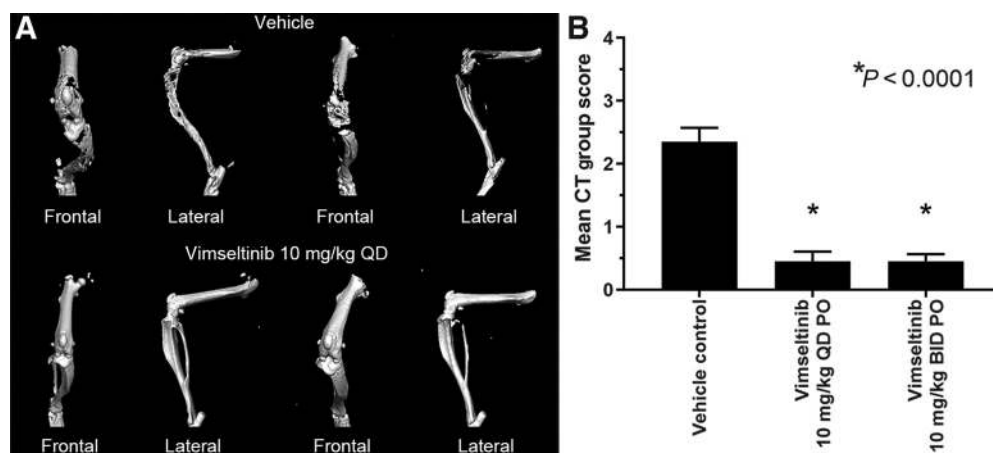
Figure 4.
Vimseltinib inhibition of bone degradation. **A,** Representative images are shown of the right hind limbs from 2 vehicle-treated mice and 2 mice treated with vimseltinib at 10 mg/kg every day in the PC3 peritibial bone invasion mouse model. **B,** Qualitative analysis of CT images of right hind limbs of all animals on study ($n = 20$/cohort).

with vehicle (Supplementary Fig. S7A). Primary tumor growth was not affected by vimseltinib in this model (Supplementary Fig. S7B).

Macrophage depletion and combination efficacy with immunotherapy

TGCT is a complex tumor with neoplastic cells expressing CSF1 representing a small component of the tumor, whereas proliferating macrophages and other CSF1R-expressing inflammatory cells make up the bulk. As such, modeling this disease is not easily done, and there is only one report of a TGCT mouse model using fresh human tumor tissue (36). Thus, measurement of the effects of vimseltinib on TAMs in a mouse cancer model as well as effects on tissue macrophages in rats were explored. To determine the effects on TAMs, as well as the impact on the adaptive immune system, the syngeneic, immunocompetent MC38 colorectal cancer model was used. All treatments were well tolerated, with mice exhibiting no weight loss or treatment-related mortalities (Supplementary Fig. S7C). Vimseltinib significantly inhibited primary tumor growth as a single agent and exhibited additive

efficacy when dosed in combination with the anti-PD1 RMP1–14 antibody (**Fig. 5A**). On day 32, single-agent vimseltinib exhibited tumor growth inhibition (%TGI) = 52% ($P < 0.0001$), anti-PD1 treatment had %TGI = 38% ($P < 0.0001$), and vimseltinib in combination with anti-PD1 exhibited %TGI = 74% ($P < 0.0001$). Five mice were sacrificed in each cohort after 3 weeks of dosing for pharmacodynamic experiments. TAMs were significantly reduced by >6-fold in the primary tumor in vimseltinib single agent ($P = 0.004$) and in combination with anti-PD1 ($P = 0.003$; **Fig. 5B**). Cytotoxic CD8$^+$ T cells increased by approximately 2-fold in the combination group (**Fig. 5C**). Although only low numbers of T_{regs} were detected in this study, they trended toward a decrease, especially in the combination group by approximately 2-fold, though this result was not statistically significant (**Fig. 5D**).

Macrophage depletion in rats

CSF1R inhibitors are known to pharmacodynamically reduce levels of macrophages in the liver (Kupffer cells) and other tissues (37).
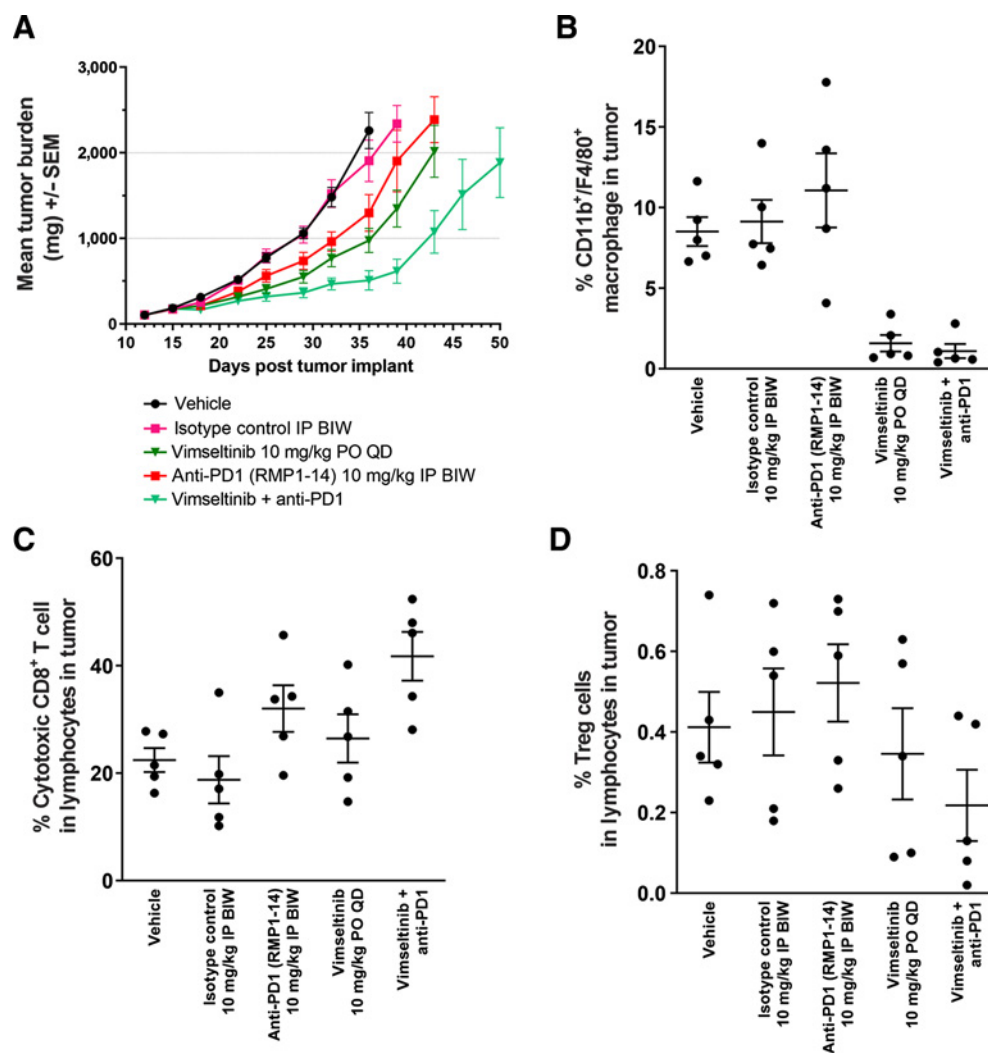

Figure 5.
Vimseltinib inhibition of tumor growth and effects on the immune system in the syngeneic MC38 colorectal cancer mouse model. **A,** Mean tumor burden of treatment groups ($n = 10$/cohort). Mice were dosed days 12–39. **B,** Levels of macrophages in excised tumors after 3 weeks of treatment. **C,** Levels of CD8$^+$ cytotoxic T cells in excised tumors after 3 weeks of treatment. **D,** Levels of Tregs in excised tumors after 3 weeks of treatment.

Vimseltinib treatment led to a statistically significant 68% decrease ($P < 0.0001$) in liver CD68$^+$ macrophages when dosed at 15 mg/kg/day in rats (Supplementary Fig. S8). CD68$^+$ macrophages were also reduced in the colon (47% decrease; $P = 0.17$).

ADME and pharmaceutical properties

In vitro and *in vivo* studies on absorption, distribution, metabolism, and excretion (ADME) and assays of other pharmaceutical properties were performed to determine the suitability of vimseltinib for human oral dosing. A crossover pharmacokinetic study in Sprague-Dawley rats showed that vimseltinib had high oral bioavailability (76% F), with volume of distribution (0.69 L/kg) and low clearance (0.03 L/hour/kg), with an elimination half-life of 14.2 hours (Supplementary Fig. S9;

Supplementary Table S3). In a Beagle dog crossover pharmacokinetic study, vimseltinib had acceptable oral bioavailability in a simple vehicle (~30% F), with volume of distribution (1.33 L/kg) and low clearance (0.15 L/hour/kg), with an elimination half-life of 6.8 hours (Supplementary Fig. S9; Supplementary Table S3). *In vitro* metabolism studies evaluated cytochrome P450 (CYP) inhibition properties. Vimseltinib exhibited IC$_{50}$ values > 75 μmol/L for all CYP isoforms studied and exhibited no time-dependent or metabolism-dependent inhibition of any CYP isoform (Supplementary Table S4), indicating a low risk for drug–drug interactions due to CYP inhibition. Vimseltinib weakly inhibited the MDR1 drug transporter (IC$_{50}$ = 4.35 μmol/L) and was a moderately weak substrate of MDR1 with an efflux ratio of 2.62 in MDCKII-MDR1 cells that decreased in the presence of the
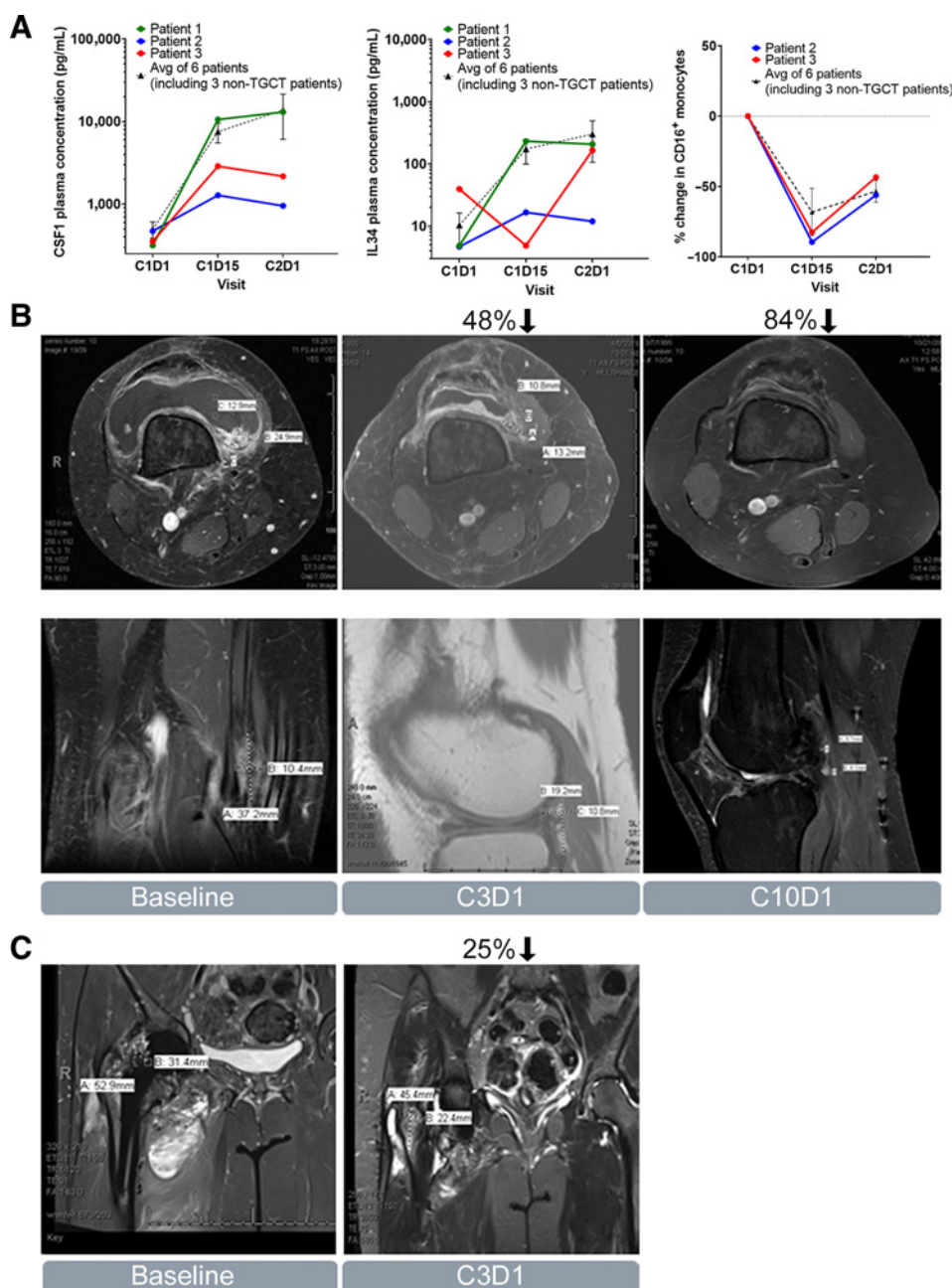

Figure 6.
Preliminary biomarker and clinical activity of vimseltinib in patients with TGCT. **A,** Increases in the CSF1R ligands CSF1 and IL34 in plasma, and decrease of levels of CSF1R-dependent nonclassical monocytes in blood in vimseltinib-treated patients. Decrease in tumor burden in patients with TGCT, in the right knee of patient 1 (**B**) and the right hip of patient 2 (**C**). Patient 3 did not consent to release of MRI images.

MDR1 inhibitor valspodar to an efflux ratio of 1.48. Vimseltinib only weakly bound the hERG channel in an *in vitro* binding assay ($EC_{50} > 25$ µmol/L, $EC_{20} = 19.4$ µmol/L) indicating a low cardiac risk for inhibition of this channel.

Translational biomarkers and clinical activity

On the basis of the compelling preclinical data indicating vimseltinib can effectively inhibit CSF1R signaling, the safety and tolerability of the drug is being tested in a first in human trial (NCT03069469; refs. 38, 39). During the dose-escalation phase of the study, 3 patients with TGCT received vimseltinib treatment with a loading dose of 30 mg once a day for 5 days followed by 30 mg twice weekly in cycles of 28 days. Radiographic response was assessed per RECIST (RECIST1.1). Circulating CSF1 and IL34 levels as well as nonclassical monocyte levels were used as biomarkers of CSF1R inhibition, all of which are known to be modulated by CSF1R inhibitors (10, 12, 14).

All 3 patients with TGCT had increases in CSF1 and IL34 levels at the end of the first cycle of treatment (cycle 2, day 1; **Fig. 6A**). Averages for the cohort of 6 patients at the same dose (including 3 patients with non-TGCT) are shown with dashed lines. A baseline blood sample was not available for patient 1, but 80%–90% decreases in circulating nonclassical monocytes were observed in the other 2 patients on cycle 1 day 15 (**Fig. 6A**). On cycle 2 day 1 at both trough and 4 hours after dose, the average plasma concentration of vimseltinib in these 3 patients was approximately 500 ng/mL (~1,200 nmol/L total drug; Supplementary Fig. S10), which is approximately the IC_{90} value for inhibition of CSF1R in a whole blood assay (**Fig. 2D**).

Patient 1 was a 23-year-old White woman with an 86.3 mm right knee TGCT, who had been treated with two prior knee surgeries. The patient had a partial response (−48%) after two cycles of treatment with further reduction after nine cycles (−84%; **Fig. 6B**). The patient withdrew consent after cycle 19. Patient 2 was a 57-year-old white woman with a 101.4 mm right hip TGCT, previously treated with six interventions including resection, hip replacement, and cryoablation. The patient had tumor shrinkage (−25%) after two cycles of treatment (**Fig. 6C**), with a deepening partial response through 12 cycles that was ongoing (−67%) after 15 cycles, as of data cutoff. Patient 3 was a 28-year-old White man with a 72 mm left knee TGCT, who had a prior resection. After two cycles of treatment, he had reduction in tumor size (−24%), but discontinued in cycle 4 due to relocation outside of the United States where the trial was being performed. The patient did not consent to publication of MRI images. There were no grade ≥3 treatment-emergent adverse events or serious adverse events reported in these 3 patients. All 3 patients had symptomatic improvements, such as pain, swelling, and range of motion, based on descriptive notes from investigators. The phase I/II expansion phase in patients with TGCT who are not amenable to surgery (Study Part 2) is ongoing.

Discussion

There is strong validation for the approach of using a CSF1R inhibitor to treat TGCT in the clinic (9, 17, 20). The use of a CSF1R inhibitor as a therapeutic for TGCT, wherein patients have serious quality of life impacts but have a normal life expectancy, stresses the need for high selectivity to reduce off-target effects. In most malignant cancers a CSF1R inhibitor would likely be used in combination with chemotherapies and/or immunotherapies, hence having fewer off-target effects would be advantageous. Vimseltinib was designed to be selective versus the closely related kinases KIT, FLT3, PDGFRA, and PDGFRB, as well as the rest of the kinome. The inhibitor potently

blocks CSF1R signaling as well as CSF1R-dependent cell proliferation and osteoclast activity. Vimseltinib is insensitive to high cellular concentrations of ATP as well as high concentrations of the ligand CSF1, which are important in the context of inhibiting tumor cell growth in TGCT. Similar to other inhibitors that induce the inactive conformation of kinases, vimseltinib exhibits slow binding inhibition of CSF1R and extended inhibition of target in cell assays after removal of drug from the assay. Vimseltinib has optimized biopharmaceutical properties for oral administration, which may be advantageous over parenteral dosing routes for anti-CSF1R antibodies. Vimseltinib significantly inhibited CSF1R signaling in pharmacokinetic/pharmacodynamic models at doses as low as 3 mg/kg orally. In efficacy models, macrophages were depleted in tumors and other tissues, and single-agent efficacy in blocking osteoclast-mediated bone degradation was observed. Single agent and combination efficacy with anti-PD1 immunotherapy in a syngeneic mouse colorectal cancer model, with effects on the adaptive immune system were also observed.

Vimseltinib is currently being evaluated in phase I/II clinical studies for the treatment of TGCT and other solid tumors as a single agent (NCT03069469) and in combination with the anti-PDL1 antibody avelumab in advanced or metastatic sarcomas (NCT04242238). In the first 3 patients with TGCT treated in the phase I trial of vimseltinib, pharmacodynamic on-target increases in plasma of the CSF1R ligands CSF1 and IL34, as well as decreases in circulating CSF1R-dependent $CD16^+$ nonclassical monocytes were detected. Concomitantly, all 3 patients showed rapid, preliminary antitumor activity by cycle 3 with deepening responses over time where evaluable. Treatment with vimseltinib was generally well tolerated in the 3 patients with TGCT, though it is premature to draw safety conclusions based on this limited dataset. Across all trials of pexidartinib in TGCT, there were five cases of serious hepatic adverse events assessed as probably drug-related out of 140 patients (20). These cases of mixed or cholestatic hepatotoxicity were rare, and the linkage, if any, to CSF1R inhibition was unclear. Pexidartinib inhibits other kinases including KIT, PDGFRA, PDGFRB, and FLT3, and is partially converted to metabolites that may contribute to hepatotoxicity (11, 21, 23). Broadly, treatment with small molecule or biologic CSF1R inhibitors results in asymptomatic increases in liver enzymes such as AST and CPK (10, 11, 24, 40, 41). This is due to an on-target mechanism of depletion of liver macrophages (Kupffer cells) which normally clear these enzymes from circulation, rather than due to hepatocyte injury (21, 37, 42). Overall, the selectivity and potency of vimseltinib, and the translational data including modulation of CSF1R-dependent biomarkers and highly encouraging antitumor activity and tolerable safety profile in patients with TGCT, supports further evaluation of vimseltinib in patients with TGCT not amenable to surgery, as well as in other indications.

Authors' Disclosures

Deciphera Pharmarceuticals outside the submitted work; in addition, W.-P. Lu has a patent for US9181223 issued. G. Tan reports personal fees and other support from Deciphera Phamaceuticals outside the submitted work. L. Vogeti reports personal fees from Deciphera Pharmaceuticals during the conduct of the study; in addition, L. Vogeti has a patent for US9,181,223 issued and a patent for US20200253973 pending. B.A. Wilky reports personal fees from Deciphera during the conduct of the study; personal fees from Daiichi Sankyo outside the submitted work. L.E. Davis reports personal fees from OncLive, Epizyme, and Daiichi outside the submitted work. M. Sharma reports personal fees from Deciphera Pharmaceuticals during the conduct of the study; personal fees from Deciphera Pharmaceuticals outside the submitted work. R. Ruiz-Soto reports personal fees from Deciphera Pharmaceuticals during the conduct of the study. D.L. Flynn reports personal fees and other support from Deciphera Pharmacueticals outside the submitted work; in addition, D.L. Flynn has a patent for US9,181,223 issued and a patent for US20200253973 pending. No disclosures were reported by the other authors.

Authors' Contributions

Acknowledgments

References

1. Wynn TA, Chawla A, Pollard JW. Macrophage biology in development, homeostasis and disease. Nature 2013;496:445–55.
2. DeNardo DG, Brennan DJ, Rexhepaj E, Ruffell B, Shiao SL, Madden SF, et al. Leukocyte complexity predicts breast cancer survival and functionally regulates response to chemotherapy. Cancer Discov 2011;1:54–67.
3. Mitchem JB, Brennan DJ, Knolhoff BL, Belt BA, Zhu Y, Sanford DE, et al. Targeting tumor-infiltrating macrophages decreases tumor-initiating cells, relieves immunosuppression, and improves chemotherapeutic responses. Cancer Res 2013;73:1128–41.
4. Wyckoff JB, Wang Y, Lin EY, Li JF, Goswami S, Stanley ER, et al. Direct visualization of macrophage-assisted tumor cell intravasation in mammary tumors. Cancer Res 2007;67:2649–56.
5. Ruffell B, Coussens LM. Macrophages and therapeutic resistance in cancer. Cancer Cell 2015;27:462–72.
6. Mun SH, Park PSU, Park-Min KH. The M-CSF receptor in osteoclasts and beyond. Exp Mol Med 2020;52:1239–54.
7. Ho J, Peters T, Dickson BC, Swanson D, Fernandez A, Frova-Seguin A, et al. Detection of CSF1 rearrangements deleting the 3′ UTR in tenosynovial giant cell tumors. Genes Chromosomes Cancer 2020;59:96–105.
8. West RB, Rubin BP, Miller MA, Subramanian S, Kaygusuz G, Montgomery K, et al. A landscape effect in tenosynovial giant-cell tumor from activation of CSF1 expression by a translocation in a minority of tumor cells. Proc Natl Acad Sci U S A 2006;103:690–5.
9. Cassier PA, Italiano A, Gomez-Roca CA, Le Tourneau C, Toulmonde M, Cannarile MA, et al. CSF1R inhibition with emactuzumab in locally advanced diffuse-type tenosynovial giant cell tumours of the soft tissue: a dose-escalation and dose-expansion phase 1 study. Lancet Oncol 2015;16:949–56.
10. Papadopoulos KP, Gluck L, Martin LP, Olszanski AJ, Tolcher AW, Ngarmchamnanrith G, et al. First-in-human study of AMG 820, a monoclonal anti-colony-stimulating factor 1 receptor antibody, in patients with advanced solid tumors. Clin Cancer Res 2017;23:5703–10.
11. Tap WD, Wainberg ZA, Anthony SP, Ibrahim PN, Zhang C, Healey JH, et al. Structure-guided blockade of CSF1R kinase in tenosynovial giant-cell tumor. N Engl J Med 2015;373:428–37.
12. Autio KA, Klebanoff CA, Schaer D, Kauh JSW, Slovin SF, Adamow M, et al. Immunomodulatory activity of a colony-stimulating factor-1 receptor inhibitor in patients with advanced refractory breast or prostate cancer: a phase I study. Clin Cancer Res 2020;26:5609–20.
13. von Tresckow B, Morschhauser F, Ribrag V, Topp MS, Chien C, Seetharam S, et al. An open-label, multicenter, phase I/II study of JNJ-40346527, a CSF-1R inhibitor, in patients with relapsed or refractory Hodgkin lymphoma. Clin Cancer Res 2015;21:1843–50.
14. Ries CH, Cannarile MA, Hoves S, Benz J, Wartha K, Runza V, et al. Targeting tumor-associated macrophages with anti-CSF-1R antibody reveals a strategy for cancer therapy. Cancer Cell 2014;25:846–59.
15. Machiels JP, Gomez-Roca C, Michot JM, Zamarin D, Mitchell T, Catala G, et al. Phase Ib study of anti-CSF-1R antibody emactuzumab in combination with CD40 agonist selicrelumab in advanced solid tumor patients. J Immunother Cancer 2020;8:e001153.
16. Razak AR, Cleary JM, Moreno V, Boyer M, Calvo Aller E, Edenfield W, et al. Safety and efficacy of AMG 820, an anti-colony-stimulating factor 1 receptor antibody, in combination with pembrolizumab in adults with advanced solid tumors. J Immunother Cancer 2020;8:e001006.
17. Cassier PA, Italiano A, Gomez-Roca C, Le Tourneau C, Toulmonde M, D'Angelo SP, et al. Long-term clinical activity, safety and patient-reported quality of life for emactuzumab-treated patients with diffuse-type tenosynovial giant-cell tumour. Eur J Cancer 2020;141:162–70.
18. Gelderblom H, Wagner AJ, Tap WD, Palmerini E, Wainberg ZA, Desai J, et al. Long-term outcomes of pexidartinib in tenosynovial giant cell tumors. Cancer 2021;127:884–93.
19. Tap WD, Gelderblom H, Palmerini E, Desai J, Bauer S, Blay JY, et al. Pexidartinib versus placebo for advanced tenosynovial giant cell tumour (ENLIVEN): a randomised phase 3 trial. Lancet 2019;394:478–87.
20. Lamb YN. Pexidartinib: first approval. Drugs 2019;79:1805–12.
21. European Medicines Agency/Committee for Medicinal Products for Human Use Assessment Report: Turalio. European Medicines Agency; 2020. p. 144.
22. Cannarile MA, Weisser M, Jacob W, Jegg AM, Ries CH, Ruttinger D. Colony-stimulating factor 1 receptor (CSF1R) inhibitors in cancer therapy. J Immunother Cancer 2017;5:53.
23. Czako B, Marszalek JR, Burke JP, Mandal P, Leonard PG, Cross JB, et al. Discovery of IACS-9439, a potent, exquisitely selective, and orally bioavailable inhibitor of CSF1R. J Med Chem 2020;63:9888–911.
24. Genovese MC, Hsia E, Belkowski SM, Chien C, Masterson T, Thurmond RL, et al. Results from a phase IIA parallel group study of JNJ-40346527, an oral CSF-1R inhibitor, in patients with active rheumatoid arthritis despite disease-modifying antirheumatic drug therapy. J Rheumatol 2015;42:1752–60.
25. Kaufman MD, Flynn DL, Ahn YM, Vogeti L, Caldwell TM. 2-aminopyrimidin-6-ones and analogs exhibiting anti-cancer and anti-proliferative activities. United States Patent and Trademark Office 2015:9,181,223 B2.
26. Zhang C, Ibrahim PN, Zhang J, Burton EA, Habets G, Zhang Y, et al. Design and pharmacology of a highly specific dual FMS and KIT kinase inhibitor. Proc Natl Acad Sci U S A 2013;110:5689–94.
27. Smith BD, Kaufman MD, Lu WP, Gupta A, Leary CB, Wise SC, et al. Ripretinib (DCC-2618) is a switch control kinase inhibitor of a broad spectrum of oncogenic and drug-resistant KIT and PDGFRA variants. Cancer Cell 2019; 35:738–51.
28. Anastassiadis T, Deacon SW, Devarajan K, Ma H, Peterson JR. Comprehensive assay of kinase catalytic activity reveals features of kinase inhibitor selectivity. Nat Biotechnol 2011;29:1039–45.

29. Fabian MA, Biggs WH 3rd, Treiber DK, Atteridge CE, Azimioara MD, Benedetti MG, et al. A small molecule-kinase interaction map for clinical kinase inhibitors. Nat Biotechnol 2005;23:329–36.

30. Spangenberg E, Severson PL, Hohsfield LA, Crapser J, Zhang J, Burton EA, et al. Sustained microglial depletion with CSF1R inhibitor impairs parenchymal plaque development in an Alzheimer's disease model. Nat Commun 2019;10: 3758.

31. Ahn YM, Clare M, Ensinger CL, Hood MM, Lord JW, Lu WP, et al. Switch control pocket inhibitors of p38-MAP kinase. Durable type II inhibitors that do not require binding into the canonical ATP hinge region. Bioorg Med Chem Lett 2010;20:5793–8.

32. Chan WW, Wise SC, Kaufman MD, Ahn YM, Ensinger CL, Haack T, et al. Conformational control inhibition of the BCR-ABL1 tyrosine kinase, including the gatekeeper T315I mutant, by the switch-control inhibitor DCC-2036. Cancer Cell 2011;19:556–68.

33. Smith BD, Kaufman MD, Leary CB, Turner BA, Wise SC, Ahn YM, et al. Altiratinib inhibits tumor growth, invasion, angiogenesis, and microenvironment-mediated drug resistance via balanced inhibition of MET, TIE2, and VEGFR2. Mol Cancer Ther 2015;14:2023–34.

34. Sato T, Yang X, Knapper S, White P, Smith BD, Galkin S, et al. FLT3 ligand impedes the efficacy of FLT3 inhibitors in vitro and in vivo. Blood 2011;117: 3286–93.

35. Manthey CL, Johnson DL, Illig CR, Tuman RW, Zhou Z, Baker JF, et al. JNJ-28312141, a novel orally active colony-stimulating factor-1 receptor/FMS-related receptor tyrosine kinase-3 receptor tyrosine kinase inhibitor with potential utility in solid tumors, bone metastases, and acute myeloid leukemia. Mol Cancer Ther 2009;8:3151–61.

36. Cheng H, Clarkson PW, Gao D, Pacheco M, Wang Y, Nielsen TO. Therapeutic antibodies targeting CSF1 impede macrophage recruitment in a xenograft model of tenosynovial giant cell tumor. Sarcoma 2010;2010:174528.

37. Radi ZA, Koza-Taylor PH, Bell RR, Obert LA, Runnels HA, Beebe JS, et al. Increased serum enzyme levels associated with kupffer cell reduction with no signs of hepatic or skeletal muscle injury. Am J Pathol 2011;179:240–7.

38. Taylor MH, Leong S, Su Y, Leary CB, Li X, Kuida K, et al. Phase 1 study of DCC-3014, an oral inhibitor of CSF1R, to assess the safety, tolerability, pharmacokinetics, and pharmacodynamics in patients with advanced solid tumors, including diffuse-type tenosynovial giant cell tumor [abstract]. In: Proceedings of the AACR-NCI-EORTC International Conference on Molecular Targets and Cancer Therapeutics; 2019 Oct 26–30; Boston, MA. Philadelphia (PA): AACR; Mol Cancer Ther 2019;18(12 Suppl):Abstract nr C087.

39. Razak A, Wilky B, Vuky J, Davis L, Bauer T, Gelderblom H, et al. Abstract 3461713: Phase 1 dose-escalation study of the safety, tolerability, pharmacokinetics, and pharmacodynamics of DCC-3014 in advanced solid tumors and tenosynovial giant cell tumor (TGCT). Connective Tissue Oncology Society Annual Meeting. 2020.

40. Sankhala KK, Blay J-Y, Ganjoo KN, Italiano A, Hassan AB, Kim TM, et al. A phase I/II dose escalation and expansion study of cabiralizumab (cabira; FPA-008), an anti-CSF1R antibody, in tenosynovial giant cell tumor (TGCT, diffuse pigmented villonodular synovitis D-PVNS). J Clin Oncol 2017;35: 11078.

41. Bendell JC, Tolcher AW, Jones SF, Beeram M, Infante JR, Larsen P, et al. A phase 1 study of ARRY-382, an oral inhibitor of colony-stimulating factor-1 receptor (CSF1R), in patients with advanced or metastatic cancers. In: Proceedings of the AACR-NCI-EORTC International Conference: Molecular Targets and Cancer Therapeutics; 2013 Oct 19–23; Boston, MA. Philadelphia (PA): AACR; Mol Cancer Ther 2013;12(11 Suppl):Abstract nr A252.

42. Wang T, Papoutsi M, Wiesmann M, DeCristofaro M, Keselica MC, Skuba E, et al. Investigation of correlation among safety biomarkers in serum, histopathological examination, and toxicogenomics. Int J Toxicol 2011;30:300–12.